https://doi.org/10.1016/j.istruc.2021.05.023

Behavior of GFRP bar reinforced geopolymer concrete filled GFRP tube columns under different loading conditions

Junaid Ahmad[a,b], Tao Yu[c], Muhammad N.S. Hadi[d,*]

[a]*PhD Candidate, School of Civil, Mining and Environmental Engineering, University of Wollongong, NSW 2522, Australia. Email: ja608@uowmail.edu.au*

[b]*Lecturer, NUST Institute of Civil Engineering (NICE), National University of Sciences and Technology (NUST), Islamabad, Pakistan.*

[c]*Professor, Department of Civil and Environmental Engineering, The Hong Kong Polytechnic University, Hung Hom, Kowloon, Hong Kong, China. Email: tao-cee.yu@polyu.edu.hk*

[d]*Associate Professor, School of Civil, Mining and Environmental Engineering, University of Wollongong, NSW 2522, Australia. Email: mhadi@uow.edu.au (*Corresponding Author)*

ABSTRACT: This paper proposes a new type of column. The glass fiber reinforced polymer (GFRP) bar reinforced geopolymer concrete (GPC) filled GFRP tube column is presented as a potential substitute of steel reinforced ordinary Portland cement concrete (OPC) column. Type of concrete (OPC and GPC), type of longitudinal reinforcement bars (steel and GFRP) and type of transverse reinforcement (steel helix and GFRP tube) were the test parameters investigated in this study. The specimens of 200 mm diameter and 800 mm height were tested under different loading conditions. Experimental load-axial deformation, load-lateral deformation and flexural load-midspan deflection of the tested specimens are presented and discussed. An equation was also proposed for the prediction of the concentric load capacity of the column. It was found that GFRP reinforcement and GFRP tube confinement resulted in a higher ductility enhancement for GPC based specimens as compared to the OPC based specimens. Also, the ductility of GFRP bar reinforced GPC or OPC filled GFRP tube columns increased with the load eccentricity. Whereas, the ductility of the steel reinforced specimens decreased with the increase of load eccentricity.

Keywords: *Geopolymer concrete; GFRP bar; GFRP tube; CFFT; Eccentric loading; Ductility; Concentric load capacity*

1. INTRODUCTION

Global warming is a threat to the sustainable future of the world [1]. Carbon dioxide (CO_2) emission is one of the key drivers of global warming. However, the production of cement involves approximately 5-7% of the CO_2 emissions [2, 3]. Portland cement is the main constituent of ordinary Portland cement concrete (OPC). It is estimated that the use of OPC in the world is almost one cubic meter per capita [4]. Also, with the increase of industrialization, the production of industrial wastes like fly ash (FA) and ground granulated blast furnace slag (GGBFS) are increasing. These industrial wastes are considered as pozzolanic in nature [4]. It is estimated that almost 75% of FA and 35% of GGBFS produced annually worldwide are wasted and not being utilized [2]. Geopolymer concrete (GPC) is known as green concrete which not only eliminates the use of Portland cement for concrete production but also utilizes the industrial wastes like fly ash and slag as binders in the GPC [5, 6]. Researchers are nowadays focused on bringing sustainability in infrastructure development through the use of GPC in structural members [5, 7-11].

Steel reinforcement replacement with fiber reinforced polymer (FRP) reinforcement is gaining attention due to long-term durability and performance of FRP reinforcement as compared to steel reinforcement. The FRP reinforcement also offers the advantages of having lighter weight, higher tensile strength and non-corrosive as compared to steel reinforcement [12]. Glass FRP (GFRP) is the most extensively used type of FRP due to its low cost. A limited number of studies have been carried out to investigate the behavior of GFRP reinforced GPC columns [8, 13]. Also, recent studies found that the use of FRP tube as transverse reinforcement in place of steel helix resulted in a more ductile and high strength structural member [14].

The concrete filled FRP tube (CFFT) column is an emerging type of construction technique since the last two decades [15, 16]. The CFFT is more attractive than the steel helix as it also has added advantages of easy construction, left-in-place formwork and better quality control

on site [14]. The concrete types like high strength concrete and geopolymer concrete are considered as more brittle than the normal strength OPC. The use of CFFT to counter the brittleness of these types of concrete was investigated by few studies [17-19]. Limited studies are found on FRP confined GPC [17, 18]. Ozbakkaloglu and Xie [20] studied the behavior of GPC filled FRP tubes. The effect of the type, thickness and shape of the FRP tube on the behavior of GPC and OPC filled FRP tubes was investigated. It was observed that the ultimate axial strains were higher for OPC and GPC filled GFRP tube as compared to the basalt FRP (BFRP) and carbon FRP (CFRP) tubes. This study was based on GPC filled FRP tubes without internal reinforcement.

The FRP bar reinforced concrete filled FRP tube (CFFT) column has recently gained significant research interest. This type of column not only provides the long-term durability but it also enhances the performance as compared to steel reinforced columns [16, 21]. Limited studies are found on the behavior of concrete filled GFRP tube columns internally reinforced with GFRP bars [21, 22].

Hadi et al. [21] conducted an experimental study to investigate the behavior of FRP reinforced concrete filled FRP tube short columns under axial concentric load, eccentric load and four-point bending. Steel reinforced concrete (RC) short columns were used as a reference. The types of FRP bar used were GFRP and CFRP. The GFRP and CFRP tubes were used as a transverse confinement in the columns. It was concluded that CFFT columns reinforced with FRP bars sustained higher axial loads, axial deformations and lateral deformations at peak load as compared to the steel reinforced reference column. Ahmed et al. [22] conducted a study to investigate the behavior of CFFT long columns reinforced with FRP bars under cyclic axial loads. The study concluded that, the ultimate strength and corresponding strain of GFRP bar reinforced concrete filled GFRP tube columns were reasonable and higher than the steel reinforced reference column. It can be observed that all the previous studies on the FRP

reinforced concrete filled FRP tube columns utilized the OPC. The GPC is a green concrete but with a higher brittleness as compared to the OPC. The use of GPC in the FRP reinforced concrete filled FRP tube columns will help in utilizing a sustainable concrete in structures and will also counter the inherit brittleness of the GPC with the added ductility provided by the external FRP tube.

This study proposes a new type of reinforced CFFT column incorporating a sustainable concrete type. This column consists of GFRP reinforced GPC filled GFRP tube column. The advantages of using this type of column are sustainability, reduction in weight of the structure, enhancement of load carrying capacity and ductility as compared to normally used steel reinforced OPC concrete columns. In this study, the general behavior, axial load-deformation and load-moment response of the GFRP bar reinforced GPC filled GFRP tube columns were experimentally investigated under concentric load, eccentric load and four-point bending.

2. EXPERIMENTAL PROGRAM

2.1 Test Matrix

The test matrix for this study is presented in Table 1. Sixteen column specimens were cast and tested. All the specimens were of 200 mm in diameter and 800 mm in height. Four groups of specimens were formed for this study. Each group was composed of four specimens. The first specimen in each group was tested under axial concentric load. The second and third specimen from each group were tested under 25 mm and 50 mm eccentric loads, respectively. The last specimen from each group was tested under flexure to ascertain the response under four-point bending.

Three letters were used to designate each group. The first letter shows the type of longitudinal reinforcement (S represent steel and G represent GFRP). The second letter shows the type of transverse reinforcement (S represent steel helix and G represent GFRP tube). The third letter is used to designate the type of concrete used where the letters O and G refer to OPC

and GPC, respectively. The numeric digits after the hyphen (-) are used to represent the different loading eccentricities. The letter F in place of the numeric digit is used for the specimens tested under four-point bending. For example, Specimen GGO-25 refer to OPC filled GFRP tube specimen internally reinforced with GFRP bars subjected to 25 mm eccentric load.

The longitudinal and cross-sectional configurations of each group are shown in Fig. 1. Groups SSO and SSG were longitudinally reinforced with six N12 steel bars and transversally with steel helix of 60 mm pitch manufactured with R10 steel bars. Groups GGO and GGG were longitudinally reinforced with six 17 mm GFRP bars and transversally confined with the GFRP tube. The volumetric reinforcement ratio of the helical confinement in the steel helix confined columns was approximately equal to the confinement ratio of the GFRP tube in the GFRP tube confined specimens. This can help in the justifiable comparison of the steel reinforced columns with the proposed column type.

2.2 Materials

2.2.1 Ordinary Portland cement concrete (OPC) and geopolymer concrete (GPC)

The ready mix OPC was procured and poured in the laboratory. The average compressive strength of the OPC was 39 MPa at 28 days tested as per AS1012.9 [23]. Geopolymer concrete cured under ambient conditions was used in this study. The optimum mix proportion proposed by Hadi et al. [24] provided a baseline. The trial tests were conducted to develop a new mix proportion with the available materials to attain the desired compressive strength and flowability. The average GPC compressive strength was 51.5 MPa at 28 days tested as per AS 1012.9 [23].

Table 2 shows the mix proportions of the GPC. The binders in the GPC mix were composed of two components (i.e. GGBFS and fly ash). The proportion of GGBFS and fly ash were 40% and 60% of the total binder content, respectively. The GGBFS for this study was

provided by the Australasian Slag Association [25]. The fly ash was provided by Boral Australia [26]. The alkaline solution in the GPC was composed of a mixture of sodium hydroxide (NaOH) solution and sodium silicate (Na_2SiO_3) solution. The ratio of NaOH to Na_2SiO_3 was 1:2.5 by mass. The superplasticizer used was MasterGlenium SKY 8700 provided by BASF chemicals Australia [27].

2.2.2 Steel reinforcement

The deformed steel bars (N12) were used for the longitudinal reinforcement of steel reinforced specimens. The steel bars used for the helix manufacturing was round steel bar R10. Tensile tests of both types of steel bars N12 and R10 were conducted as per AS 1391-07 [28]. The average tensile strengths of N12 deformed and R10 plain steel bars were 650 MPa and 500 MPa, respectively.

2.2.3 Glass fiber reinforced polymer (GFRP) longitudinal reinforcement

The reinforcement used in this study was spirally wounded GFRP bars of 17 mm diameter. The GFRP bars were supplied by Domeshells Australia [29]. The average tensile strength and elastic modulus of GFRP bars were 749 MPa and 36.8 GPa, respectively, as per ASTM D7205/D7205M-11 [30]. The average tensile properties of the GFRP bars are quite close to the values reported by He et al. [31] and Qu et al. [32]. The average compressive strength and elastic modulus of the tested GFRP bar specimens were 472 MPa and 39.1 GPa, respectively, as per ASTM D695-15 [33]. The relationship of compressive and tensile strength of the tested GFRP bars is almost similar to the results presented by Hadi et al. [21]. The ratio of compressive to tensile modulus of elasticity is 1.06. A similar ratio was previously reported in AlAjarmeh et al. [34], which testify the test results presented in this study.

2.2.4 Glass fiber reinforced polymer (GFRP) tube

All the GFRP tubes used in this study were of 200 mm internal diameter and wall thickness of 1.5 mm. The winding angle of the glass fibers in the tube was $\pm 78^{o}$ to the longitudinal direction

of the tube, as per the manufacturer provided data. The tensile characteristics of the tube were determined in both the hoop and longitudinal directions. The tensile properties of the tube in the circumferential direction were determined using a split disk test, as per ASTM D2290-08 [35]. The test sample was 35 mm wide. Two reduced widths were created 180^{o} apart. The reduced width was created with the help of 8 mm radius notches at both ends of the sample. Two strain gauges of gauge length 20 mm were attached at the two opposite reduced areas of the test samples. The test was conducted using the Instron Universal testing machine (capacity= 500kN) at a displacement controlled loading rate of 2 mm/min. The hoop tensile strength and strain at failure were 701 MPa and 1.6%, respectively. The GFRP coupon test was conducted as per ASTM D3039/D3039M-14 [36] to determine the tube properties in the longitudinal direction. The width and length of the test coupons were 25 mm and 250 mm, respectively. The average tensile strength of the GFRP tube in the longitudinal direction was measured as 20.2 MPa. The longitudinal tensile strength is considerably lower than the circumferential tensile strength of the GFRP tube. This can be due to the reason that the majority of the fibers are oriented in the circumferential direction of the tube and thus resulted in a higher tensile strength in the circumferential direction.

2.3 Specimen fabrication

For steel reinforced specimens, the steel longitudinal reinforcement bars were tied to the steel helix at the design locations. A plastic template was used to keep the longitudinal bars at the designed location and a steel template was used to keep a constant pitch throughout the reinforcement cage. Small pieces of steel were welded at the bottom and sides of the reinforcement cage to provide the 20 mm cover. The prepared steel reinforcement cage was placed in the GFRP tube which acted as a formwork. The GFRP tube on the steel reinforced specimens were cut after 28 days and was only used as a formwork.

177 For GFRP bar reinforced concrete filled GFRP tube specimens, the GFRP bars were tied
178 with two steel hoops one at the top and at the bottom to keep the bars at the same distance from
179 each other. The diameter of the round steel bar used to prepare the steel hoop was 6 mm. Steel
180 hoops were placed so as to avoid any addition to strength. Also a plastic template with holes
181 of the size of GFRP bar diameter was used to keep the bars at the design locations. A cover of
182 20 mm was provided for the GFRP bars. The prepared GFRP bar cages were placed in the
183 GFRP tubes for Groups GGO and GGG. The tubes were fixed on a wooden pallet with the
184 glue. The straightness was checked with a plumb line bubble level.

185 The OPC was supplied in a truck mixer to the laboratory. The OPC was then placed into
186 the molds manually using aluminum scoops. A poker vibrator was used to avoid air traps and
187 allow proper placement of concrete in the molds. The top surface of the specimens was finished
188 and levelled. After 24 hours, wet hessian was placed on the specimens for curing for 28 days.

189 The GPC was prepared in the laboratory using a rotating drum mixer with a mixing
190 capacity of 0.1 m^3. Sodium hydroxide solution was prepared about 18-20 hours before the
191 concrete mixing. Sodium silicate was added to the sodium hydroxide solution 35-40 minutes
192 before mixing to prepare the alkaline solution. Coarse aggregates, sand, fly ash and GGBFS
193 were mixed thoroughly in the mixer first. Alkaline solution was then added to the mix.
194 Afterwards, the water and superplasticizer were added to the mix. The prepared GPC was then
195 poured into the molds. Similar to the OPC pouring, a poker vibrator was used to remove the
196 air traps. After pouring, the top surface of the specimens were finished and covered with a
197 polyethylene sheet to reduce the loss of moisture. The polyethylene sheet was removed after
198 28 days.

199 **2.4 Test setup and procedure**

200 The concentrically loaded specimens were instrumented to record the load and the axial
201 deformation. The eccentrically loaded specimens were instrumented to obtain the load, the

axial deformation and the lateral deformation. The specimens tested under four-point bending were instrumented to record the load and the midspan deflection.

A 5000 kN compression testing machine was used for all the tests at the Civil Engineering High bay laboratory, University of Wollongong, Australia. To avoid the failure at the top and the bottom of the specimens, CFRP strips of width 100 mm were wrapped in two layers using the epoxy resin. In addition, the top surface of the specimens was capped with a uniform layer of high strength plaster. The axial deformation in all the specimens was recorded using two linear variable displacement transducers (LVDTs) positioned at the two opposite corners of the testing machine. The lateral deformation at the mid height of the eccentrically loaded specimens was recorded using a laser triangulation. For all the concentric and eccentric loading tests, the loading heads and test setup were the same as previously reported by Hadi et al. [37]. Figure 2 shows the test setup for different loading types. The specimens were preloaded to avoid the misalignment during the test setup at a loading rate of 50 kN/min up to 100 kN. The specimens were then unloaded to 20 kN at the same loading rate. Afterwards, a displacement controlled loading rate of 0.3 mm/min was used to test all the concentric and eccentric loaded specimens.

The specimens were wrapped at both ends with CFRP sheet to avoid failure in the shear zone under four-point bending. The distance between the two bottom load points was 700 mm and the distance between the two top supports was 230 mm. The distance of the top support from the nearest bottom load point was 235 mm. A hole was provided at the center of the bottom rig to allow the use of a laser triangulation for the measurement of midspan deflection. The specimens tested under four-point bending were also preloaded at a loading rate of 50 kN/min up to 50 kN. A similar loading rate was then used to unload the specimens to 20 kN. Afterwards, a displacement controlled loading rate of 0.3 mm/min was used to test all the specimens under four-point bending.

3. RESULTS AND DISCUSSION

Table 3 and Table 4 show the test results. The axial load-deformation behavior, peak axial loads and ductility of the tested specimens are presented and discussed below. The effects of longitudinal reinforcement (steel and GFRP), transverse reinforcement (steel helix and GFRP tube), type of concrete (OPC and GPC), and eccentricity on peak axial load and ductility of the tested specimens are also discussed. The failure modes of the tested specimens are shown in Fig. 3 and Fig. 4. The axial load-axial deformation behavior of the specimens tested under concentric and eccentric axial loads was recorded under monotonic axial compression till failure. Figures 5, 6 and 7 represent the axial load-axial deformation response of the specimens tested under concentric, 25 mm eccentric and 50 mm eccentric axial compression, respectively. The load-midspan deflection behavior of the specimens tested under four-point bending is shown in Fig. 8.

The ratio of ultimate deformation (δ_u) to yield deformation (δ_y) was used to calculate the ductility index (μ) of the tested specimens. Equation (1) shows the formula to determine the ductility index of the tested specimens.

$$\mu = \frac{\delta_u}{\delta_y} \quad (1)$$

Figure 9 shows the location of yield and ultimate deformations on a typical load-deformation curve for the tested specimens. A best fit regression line was plotted on the first linear branch of the axial load-axial deformation curve of the tested specimens. A horizontal line at the peak axial load at the end of the second branch was also plotted. The intersection of these two lines was assumed to be the yield point and the deformation corresponding to this point was used as the yield deformation (δ_y). The point at the 85% of the peak axial load in the third branch was assumed to be the ultimate point and the deformation corresponding to this point was considered as the ultimate deformation (δ_u). A similar approach for the calculation of yield and ultimate deformation has already been adopted by Hadi et al. [21].

3.1 Failure modes

The failure modes of the tested specimens are shown in Fig. 3 and Fig. 4. It was observed that in concentrically loaded steel reinforced specimens, cracks started to be visible on the concrete surface near the peak load. At the peak load, the concrete cover fell off from the specimen and exposed the core of the specimen. Also, the longitudinal steel bars started to buckle. The steel helix continued to hold the longitudinal steel bars. Rupture of the steel helix and crushing of the concrete resulted in the failure of the steel reinforced specimens. It was also observed that the concrete cracking pattern was more extensive and resulted in spalling of concrete cover throughout the specimen in case of Group SSO as compared to Group SSG. This is due to the fact that the GPC have higher tensile and bond strength as compared to the OPC. In the eccentrically loaded steel reinforced specimens, the concrete on the compression side crushed and tension cracks developed on the tension face. The failure was resulted due to buckling and rupture of the longitudinal steel bars on the compression and tension face, respectively. The failure of the steel reinforced specimens under four-point bending initiated due to the crushing of concrete at the top and tension cracks at the bottom as shown in Fig. 4. Afterwards, the buckling of steel bars in compression and rupture of steel bars in tension resulted in the failure of the specimens.

For all the specimens in Groups GGO and GGG, the failure was initiated with loud sounds of the rupture of the GFRP bars in compression. Also, minor rupture cracks started to appear on the GFRP tube. Later, the failure of all the specimens occurred due to the full rupture of the GFRP tube at the point of maximum stress. Also, it can be observed from Fig. 3 that as the eccentricity of the specimens increased, the failure location moved from mid-height to the top or bottom third portions of the specimens. For Specimens GGO-F and GGG-F, the failure was initiated with the FRP bar rupture inside and afterwards the rupture of the BFRP tube resulted in the complete failure of the specimens as shown in Fig. 4.

3.2 Axial load-deformation behavior

Steel reinforced specimens in Groups SSO and SSG resulted in three branches of the axial load-axial deformation curve as can be seen in Figs. 5, 6 and 7. The first branch was linear and controlled by the concrete only. The behavior of Group SSO was similar to Group SSG initially during the first branch. At the peak load, the second branch of the curve was initiated. At the peak load, the concrete cover fell off and the area of the concrete reduced to the core only. This resulted in a reduction of load. The reduction of load recorded for Group SSG was higher than Group SSO. This can be due to the brittle nature of GPC which resulted in a sharp reduction of load at the peak load. In the third branch, the load started to reduce with the increase in axial deformation. The third branch was controlled by the concrete core, steel longitudinal reinforcement and transverse steel helix. It was also observed that a longer cracking and spalling pattern was visible for Group SSO than Group SSG. This behavior can be justified with the fact that the GPC has higher tensile and bond strengths than OPC [38-40]. The steel reinforced specimens under eccentric loads experienced failure due to the cracks in concrete on the tension face, longitudinal steel bar buckling at the compression face and longitudinal steel bar rupture at the tension face of the specimens.

The axial load-axial deformation behavior of Groups GGO and GGG can also be divided into three main branches as shown in Figs. 5, 6 and 7. The first branch was linear and controlled by the concrete compression in the tube till the compressive strength of the concrete. At the concrete compressive strength, the second linear branch of the curve was initiated for Groups GGO and GGG. A difference in the behavior of Groups GGG and GGO was noticed during transition between the first and the second branches for concentrically loaded specimens. For Specimen GGG-0, the load-deformation curve resulted in a sudden drop at the transition point and then started to increase. Whereas, Specimen GGO-0 did not experience the drop of load at the end of the first branch. A similar drop of load at the transition point has already been

observed for the FRP confined high strength OPC by Oliveira et al. [41]. This similarity of the behavior suggested that the FRP confined GPC behavior is quite similar to the FRP confined high strength OPC under axial compressive loads. This can be due to the higher brittleness of GPC and high strength OPC than normal strength OPC, which could have caused the sudden crushing of concrete. In the second branch, the load increased with the axial deformation till the rupture of GFRP tube. The second branch was controlled by the GFRP longitudinal bars and external GFRP tube. The third branch started at the peak axial load where the GFRP tube started to rupture. This resulted in a sharp drop in the axial load-axial deformation curve in the third branch of the curve.

3.3 Load-midspan deflection behavior

The load-midspan deflection curves of the tested specimens can be divided into two main branches as shown in Fig. 8. For the steel reinforced specimens, the first branch was till the peak load. The tension cracks at the bottom and crushing of concrete at the top started in the first branch. At the peak load, the concrete at the top crushed and the tension cracks opened up. After the peak load, the second branch started and ended at the failure of the specimens due to the rupture of the longitudinal steel bar. For the GFRP tube confined specimens, the first branch of the curve ended with the sudden drop of load at the peak load. The concrete in the tube crushed at top and tension cracks developed at bottom during the first branch. The GFRP tube ruptured at the peak load. During the second branch, after the load drop, the FRP reinforcement carried the flexural load and resulted in a slight increase of load. The second branch ended with the GFRP bar and tube rupture which in turn resulted in the specimen failure.

3.4 Peak axial load and ductility of specimens tested under concentric loads

The test results of the specimens tested under concentric loads are presented in Table 3. It can be observed from Table 3 that Specimen SSG-0 resulted in a 34.3% higher peak axial load than Specimen SSO-0. This difference is due to the higher unconfined strength of GPC than OPC.

326 The ductility index of Specimen SSG-0 was 26.2% lower than Specimen SSO-0. This result is
327 in line with the observations made by other studies regarding brittleness of GPC, for example
328 Steinerova et al. [42].

329 It can also be observed from the test results that the peak axial load of Specimen GGG-0
330 was 13.2% lower than Specimen GGO-0. This can be due to the fact that the effectiveness of
331 FRP confinement reduces with the increase in unconfined concrete strength [43, 44]. It has
332 already been mentioned that the unconfined concrete strength of GPC was higher than the OPC.
333 Therefore the increase of the capacity due to the FRP tube confinement is more pronounced in
334 case of OPC based specimen as compared to the GPC based specimen. A similar observation
335 of reduced confined strength with the increase in unconfined concrete strength was made by
336 Mandal et al. [44]. The ductility index of Specimen GGG-0 was also 9% lower than Specimen
337 GGO-0. This can be due to the higher brittleness of GPC than OPC [42].

338 Specimen GGO-0 showed 81.7% and 53.6% higher peak axial load and ductility index,
339 respectively than Specimen SSO-0. Similarly, Specimen GGG-0 resulted in 17.3% and 89.4%
340 higher peak axial load and ductility index than Specimen SSG-0, respectively. Considering that
341 the two types of specimens had almost a similar volume ratio of transverse reinforcement, this
342 shows the superior performance of GFRP bar reinforced and GFRP tube confined specimens
343 than the steel reinforced specimens. Also, it can be noticed that the ductility enhancement in
344 the GPC specimens (i.e. from SSG-0 to GGG-0) was greater than the OPC specimens (i.e. from
345 SSO-0 to GGO-0). The peak axial load enhancement due to GFRP tube confinement was higher
346 for OPC specimens (i.e. from SSO-0 to GGO-0) than GPC specimens (i.e. from SSG-0 to
347 GGG-0).

348 **3.5 Peak axial load and ductility of specimens tested under eccentric loads**

349 Figure 6 shows the axial load-axial deformation and axial load-lateral deformation behavior of
350 the specimens tested under 25 mm eccentric loads. Specimen SSO-25 showed a 21.5% lower

351 peak axial load than Specimen SSG-25. This lower peak axial load of Specimen SSO-25 was
352 due to the lower unconfined concrete strength of OPC than GPC in this study. On the contrary,
353 the ductility index of Specimen SSO-25 was 36.6% higher than Specimen SSG-25.
354 Specimen GGG-25 resulted in 3.4% lower peak axial load than Specimen GGO-25. Also,
355 the ductility index of Specimen GGG-25 was 5.9% lower than Specimen GGO-25. Specimen
356 GGG-25 resulted in 12.2% higher peak axial load and 207% higher ductility index than
357 Specimen SSG-25. Similarly, Specimen GGO-25 resulted in 47.3% higher peak axial load and
358 139% higher ductility index than Specimen SSO-25. It can be observed that the peak axial load
359 enhancement was greater in OPC specimens (i.e. from SSO-25 to GGO-25) than GPC
360 specimens (i.e. from SSG-25 to GGG-25). However, the ductility enhancement was more
361 significant for the GPC specimens (i.e. from SSG-25 to GGG-25) than OPC specimens (i.e.
362 from SSO-25 to GGO-25).
363 The axial load-axial deformation and axial load-lateral deformation curves of the
364 specimens tested under 50 mm eccentric loads are shown in Fig. 7. Specimen SSO-50 resulted
365 in a 22.6% lower peak axial load than Specimen SSG-50. Whereas, the ductility index of
366 Specimen SSO-50 was 17.9% higher than Specimen SSG-50 due to the brittle behavior of
367 GPC.
368 Specimen GGG-50 experienced a 5.6% and 0.28% lower peak axial load and ductility
369 index, respectively than Specimen GGO-50. Specimen GGO-50 resisted 63% higher peak axial
370 load than Specimen SSO-50. A major difference in ductility of Specimens GGO-50 and SSO-
371 50 can be observed. Specimen GGO-50 showed a ductility index which was almost four times
372 the ductility index of Specimen SSO-50. Similarly, the peak axial load experienced by
373 Specimen GGG-50 was 19% higher than Specimen SSG-50. The ductility index of Specimen
374 GGG-50 was approximately 4.7 times the ductility index of Specimen SSG-50. This shows the
375 GFRP bar reinforcement and GFRP tube confinement has a major effect on the peak axial load

and ductility enhancement compared to the steel reinforced and steel helix confined specimens under higher eccentric axial loads.

3.6 Peak load and ductility of specimens tested under under flexural loads

The peak flexural load, midspan deflection at peak flexural load and ductility index of the tested specimens are tabulated in Table 4. It can be observed that the peak flexural load of Specimen SSG-F was 2.5% higher than Specimen SSO-F. Also, the ductility index of Specimen SSG-F was 20.8% lower than Specimen SSO-F. This can be due to the brittle nature of GPC than OPC. Specimen SSG-F experienced a sharp decline of flexural load after the peak as compared to Specimen SSO-F. Specimens GGG-F and GGO-F resulted in higher peak flexural loads than steel reinforced Specimens SSG-F and SSO-F, respectively. Also, the ductility index of Specimens GGG-F and GGO-F was significantly lower than Specimens SSG-F and SSO-F, respectively. Specimen GGG-F resulted in 42.6% lower peak flexural load than Specimen GGO-F and the ductility index of Specimen GGO-F was 24.7% lower than Specimen GGG-F.

3.7 Effect of longitudinal reinforcement and transverse confinement

Two types of longitudinal reinforcement (i.e. steel and GFRP) and transverse confinement (i.e. steel helix and GFRP tube confinement) were used in this study. In Fig. 10, the effect was plotted in terms of normalized peak axial load and normalized ductility index. The results of GFRP bar reinforced GFRP tube confined specimens were normalized based on the steel reinforced counterparts. Figure 10 shows that for all the types of concrete and the load eccentricities, the GFRP bar reinforced GFRP tube confined specimens showed higher peak axial load and higher ductility than the steel reinforced specimens. Also it can be observed that the ductility enhancement due to GFRP bar reinforcement and GFRP tube confinement was more pronounced at higher load eccentricities than the peak axial load enhancement.

3.8 Effect of concrete type

The effect of concrete type on the peak axial load and ductility index of the tested specimens is shown in Fig. 11. It can be observed that for all the load eccentricities, steel reinforced OPC specimens resulted in lower peak axial load and higher ductility than the steel reinforced GPC specimens. This is due to the lower unconfined strength of OPC and higher brittleness of GPC.

Figure 11 also shows that for all eccentricities, the GFRP bar reinforced OPC filled GFRP tube confined specimens resulted in higher peak axial load and ductility index than the GFRP bar reinforced GPC filled GFRP tube confined specimens. The difference of peak axial load and ductility index between the OPC and GPC specimens was not as significant as in steel reinforced specimens. This showed that the GFRP tube confinement effectively countered the brittleness of GPC and brought the GPC specimens close in performance to the OPC specimens.

3.9 Effect of eccentricity

Figure 12 shows the effect of load eccentricity on the peak axial load and ductility index of the tested specimens. It can be observed that for all the types of specimens tested, the peak axial load decreased with an increase in the load eccentricity. The ductility of steel reinforced specimens, irrespective of the type of concrete used, decreased with the load eccentricity. The decrease in ductility with eccentricity for steel reinforced OPC specimens was slightly higher than the steel reinforced GPC specimens. The ductility of GFRP bar reinforced GFRP tube confined specimens increased with the load eccentricity. This increase in ductility is independent of the type of concrete used. Also it can be observed that the increase in ductility in GFRP bar reinforced GFRP tube confined specimens with eccentricity was slightly higher for the GPC filled specimens than the OPC filled specimens. This shows the ductility performance of GFRP bar reinforced GPC filled GFRP tube specimens improved under higher load eccentricities.

4. THEORATICAL LOAD PREDICTIONS

The concentric load capacity of the GFRP reinforced concrete filled GFRP tube column can be predicted using Eq. (2). A similar form of equation was used in Khan et al. [16].

$$P = 0.85f'_{cc}\left(A_g - A_b\right) + \alpha f_b A_b \quad (2)$$

Where f_{cc}' and f_b are the confined concrete strength and the ultimate tensile strength of the FRP bar, respectively; A_g and A_b are the gross cross-sectional area of the column and the total area of the FRP bars, respectively. The factor α is the reduction factor to account for the lower compressive strength of the FRP bar as compared to its tensile strength. The value of α was taken as 0.35 based on Afifi et al. [45]. The f_{cc}' was calculated based on different confinement models available in the literature. The average unconfined concrete strength during the test duration was used in the calculation of f_{cc}'. Table 5 shows the concentric load carrying capacities of Specimens GGO-0 and GGG-0 calculated using ACI 440.2R-08 [46], Benzaid et al. [47], Harries and Kharel [48], Wu et al. [49], Youssef et al. [50], Samaan et al. [51], Toutanji [52], Lam and Teng [53] and Teng et al. [54].

It can be observed from Table 5 that except Toutanji [52] all the existing confinement models compared in this study were able to conservatively predict the concentric load carrying capacity of Specimen GGO-0. However, ACI 440.2R-08 [46], Benzaid et al. [47], Harries and Kharel [48], Wu et al. [49] and Youssef et al. [50] were able to predict the concentric load capacity of both Specimens GGO-0 and GGG-0, conservatively. The ratio of the predicted values to the experimental load carrying capacities (P/P_{exp}) calculated using Eq. (2) ranged from 0.75 to 1.26. Also, the confinement model proposed by ACI 440.2R-08 [46] resulted in the least mean absolute percentage error (MAPE) with the conservative load carrying capacity prediction for both Specimens GGO-0 and GGG-0. It can also be concluded that the load contribution of the GFRP bars in the axial load carrying capacity of the GFRP reinforced concrete filled GFRP tube columns should not be ignored for accurate predictions.

5. CONCLUSIONS

The following conclusions are drawn based on the results and discussion:

1. The GFRP bar reinforced GPC filled GFRP tube specimens resulted in higher peak axial loads and ductility index than the steel reinforced GPC reference specimens. Similarly, the GFRP bar reinforced OPC filled GFRP tube specimens resulted in higher peak axial loads and ductility index than the steel reinforced OPC reference specimens.
2. For all eccentricities, the ductility enhancement for the GPC based specimens (i.e. from SSG to GGG) was higher than the OPC based specimens (i.e. from SSO to GGO) when the steel helix was replaced with GFRP tube and steel bars were replaced with GFRP bars. On the contrary, the peak axial load enhancement for the OPC based specimens was higher than the GPC based specimens.
3. The effect of concrete type on the peak axial loads and ductility was significantly reduced in the GFRP reinforced concrete filled GFRP tube specimens than the steel reinforced specimens.
4. The peak axial loads of all the axially tested specimens decreased with the eccentricity. Irrespective of the type of concrete, the ductility of the steel reinforced specimens decreased with the eccentricity, whereas, the ductility of GFRP bar reinforced CFFT specimens increased with the eccentricity. Therefore, it can be concluded that the GFRP bar reinforced concrete filled GFRP tube specimens performs better under load eccentricity than the steel reinforced concrete specimens.
5. The concentric load capacity of the GFRP reinforced concrete filled GFRP tube columns can be predicted using the existing confinement models. The confinement model recommended in ACI 440.2R-08 [46] resulted in the least MAPE and conservative predictions for the concentric load capacity of the column.

Finally, for sustainable construction, the use of GFRP bar reinforced GPC filled GFRP tube column can be recommended as its strength and ductility performance is comparable to the GFRP bar reinforced OPC filled GFRP tube columns.

ACKNOWLEDGEMENT

The authors would like to acknowledge the financial support provided by the Australian Government through the Australian Research Council's Discovery Projects funding scheme (project ID: DP170102992). The authors are also grateful to Boral Australia, Australasian Slag Association (ASA), BASF chemicals Australia and Domeshells Australia for providing the fly ash, GGBFS, superplasticizer and GFRP reinforcement, respectively for this study. Also thanks to the technical staff at the Civil Engineering High Bay Labs, University of Wollongong, Australia for their continuous support during experimental work especially Mr. Ritchie Mclean. The first author would also like to acknowledge the Higher Education Commission (HEC) Pakistan and the University of Wollongong, Australia for his PhD scholarship support.

REFERENCES

[1] Luhar S, Cheng T-W, Luhar I. Incorporation of natural waste from agricultural and aquacultural farming as supplementary materials with green concrete: A review. Compos B: Eng. 2019;175:107076.

[2] Gholampour A, Ozbakkaloglu T, Ng C-T. Ambient- and oven-cured geopolymer concretes under active confinement. Constr Build Mater. 2019;228:116722.

[3] Ali S, Sheikh MN, Hadi MNS. Influence of Polypropylene and Glass Fibers on Alkali-Activated Slag/Fly Ash Concrete. ACI Struct J.2020;117(4):183-92.

[4] Jindal BB. Investigations on the properties of geopolymer mortar and concrete with mineral admixtures: A review. Constr Build Mater. 2019;227:116644.

[5] Farhan NA, Sheikh MN, Hadi MNS. Behavior of Ambient-Cured Geopolymer Concrete Columns under Different Loads. ACI Struct J. 2018;115(5):1419-29.

[6] Ahmad J, Yu T, Hadi MNS. Basalt fiber reinforced polymer (BFRP) confined geopolymer concrete. ACI Struct J. 2021;118(1):289-300.

[7] Junaid MT, Elbana A, Altoubat S, Al-Sadoon Z. Experimental study on the effect of matrix on the flexural behavior of beams reinforced with Glass Fiber Reinforced Polymer (GFRP) bars. Compos Struct. 2019;222:110930.

[8] Maranan GB, Manalo AC, Benmokrane B, Karunasena W, Mendis P. Behavior of concentrically loaded geopolymer-concrete circular columns reinforced longitudinally and transversely with GFRP bars. Eng. Struct. 2016;117:422-36.

[9] Farhan NA, Sheikh MN, Hadi MNS. Behaviour of Ambient Cured Steel Fibre Reinforced Geopolymer Concrete Columns Under Axial and Flexural Loads. Structures. 2018;15:184-95.

[10] Junaid MT, Elbana A, Altoubat S. Flexural response of geopolymer and fiber reinforced geopolymer concrete beams reinforced with GFRP bars and strengthened using CFRP sheets. Structures. 2020;666-77.

[11] Zhou Z, Wang T, Hui C, Li J. Seismic performance evaluation of assembled GCFST column-section steel beam frames with geopolymer concrete walls. Structures. 2020;2537-48.

[12] AlAjarmeh OS, Manalo AC, Benmokrane B, Karunasena W, Mendis P. Effect of spiral spacing and concrete strength on behavior of GFRP-reinforced hollow concrete columns. J. Compos Constr. 2020;24(1):04019054.

[13] Elchalakani M, Karrech A, Dong M, Mohamed Ali MS, Yang B. Experiments and Finite Element Analysis of GFRP Reinforced Geopolymer Concrete Rectangular Columns Subjected to Concentric and Eccentric Axial Loading. Structures. 2018;14:273-89.

[14] Wei Y, Zhang X, Wu G, Zhou Y. Behaviour of concrete confined by both steel spirals and fiber-reinforced polymer under axial load. Compos Struct. 2018;192:577-91.

[15] Fam A, Rizkalla SH. Behavior of axially loaded concrete-filled circular FRP tubes. ACI Struct J. 2001;98(3):280-9.

[16] Khan QS, Sheikh MN, Hadi MN. Axial-flexural interactions of GFRP-CFFT columns with and without reinforcing GFRP bars. J. Compos Constr. 2016;21(3):04016109.

[17] Lokuge W, Karunasena W. Ductility enhancement of geopolymer concrete columns using fibre-reinforced polymer confinement. J. Compos Mater. 2015;50(14):1887-96.

[18] Nagan S, Karthiyaini S. A Study on Load Carrying Capacity of Fly Ash Based Polymer Concrete Columns Strengthened Using Double Layer GFRP Wrapping. Adv. Mater Sci. Eng. 2014;2014:1-6.

[19] Ozbakkaloglu T, Vincent T. Axial Compressive Behavior of Circular High-Strength Concrete-Filled FRP Tubes. J. Compos Constr. 2014;18(2):04013037.

[20] Ozbakkaloglu T, Xie T. Geopolymer concrete-filled FRP tubes: Behavior of circular and square columns under axial compression. Compos B: Eng. 2016;96:215-30.

[21] Hadi MNS, Khan QS, Sheikh MN. Axial and flexural behavior of unreinforced and FRP bar reinforced circular concrete filled FRP tube columns. Constr Build Mater. 2016;122:43-53.

[22] Ahmed AA, Hassan M, Mohamed H, Abouzied A, Masmoudi R. Axial behavior of circular CFFT long columns internally reinforced with steel or carbon and glass FRP longitudinal bars. Eng Struct. 2018;155:267-78.

[23] AS. Methods of Testing Concrete–Compressive Strength Tests–Concrete, Mortar and Grout Specimens. Standard Australia. 2014. AS 1012.9..

[24] Hadi MNS, Farhan NA, Sheikh MN. Design of geopolymer concrete with GGBFS at ambient curing condition using Taguchi method. Constr Build Mater. 2017;140:424-31.

[25] ASA. Ground Granulated Blast Furnace Slag (GGBFS). Australasian (iron & steel) Slag Association (ASA). accessed August 01, 2019. www.asa-inc.org.au/products/ground-granulated-blast-furnace-slag.

[26] Boral Australia. Fly ash (bagged). accessed August 01, 2019. https://www.boral.com.au/products/cementitious-materials/fly-ash/fly-ash-bagged

549 [27] BASF chemicals Australia. MasterGlenium SKY 8700. accessed August 01, 2019.
550 www.master-builders-solutions.basf.com.au/en-au/products/mastergleniumsky/mastergleniu
551 m-sky-8700.
552 [28] AS. Metallic materials – Tensile testing at ambient temperature. Standard Australia. 2007.
553 AS 1391-07.
554 [29] Domeshells Australia. Composite materials for dome construction. accessed August 01,
555 2019. https://www.domeshells.com.au.
556 [30] ASTM. Standard test method for tensile properties of fiber reinforced polymer matrix
557 composite bars. 2011. ASTM D7205-11. West Conshohocken, PA.
558 [31] He J, Liu Y, Chen A, Dai L. Experimental investigation of movable hybrid GFRP and
559 concrete bridge deck. Constr Build Mater. 2012;26(1):49-64.
560 [32] Qu W, Zhang X, Huang H. Flexural Behavior of Concrete Beams Reinforced with Hybrid
561 (GFRP and Steel) Bars. J. Compos Constr. 2009;13(5):350-9.
562 [33] ASTM. Standard test method for compressive properties of rigid plastics. 2015. ASTM
563 D695-15. West Conshohocken, PA.
564 [34] AlAjarmeh O, Manalo A, Benmokrane B, Vijay P, Ferdous W, Mendis P. Novel testing
565 and characterization of GFRP bars in compression. Constr Build Mater. 2019;225:1112-26.
566 [35] ASTM. Standard test method for apparent hoop tensile strength of plastic or reinforced
567 plastic pipe by split disk method. 2008. ASTM D2290. West Conshohocken, PA.
568 [36] ASTM. Standard test method for tensile properties of polymer matrix composite materials.
569 2014. ASTM D3039/D3039M-14. West Conshohocken, PA.
570 [37] Hadi MNS, Ahmad J, Yu T. Investigation of BFRP bar reinforced geopolymer concrete
571 filled BFRP tube columns. Proc. Inst. Civil Eng. – Struct. Build. 2020;0(0):1-41.
572 [38] Fernandez-Jimenez AM, Palomo A, Lopez-Hombrados C. Engineering properties of
573 alkali-activated fly ash concrete. ACI Mater J. 2006;103(2):106.

574 [39] Sarker PK, Haque R, Ramgolam KV. Fracture behaviour of heat cured fly ash based
575 geopolymer concrete. Mater Design. 2013;44:580-6.
576 [40] Sofi M, Van Deventer J, Mendis P, Lukey G. Bond performance of reinforcing bars in
577 inorganic polymer concrete (IPC). J. Mater Sci. 2007;42(9):3107-16.
578 [41] Oliveira DSd, Raiz V, Carrazedo R. Experimental Study on Normal-Strength, High-
579 Strength and Ultrahigh-Strength Concrete Confined by Carbon and Glass FRP Laminates. J.
580 Compos Constr. 2019;23(1):04018072.
581 [42] Steinerova M, Matulova L, Vermach P, Kotas J. The Brittleness and Chemical Stability
582 of Optimized Geopolymer Composites. Mater. 2017;10(4):396.
583 [43] Lim JC, Ozbakkaloglu T. Confinement Model for FRP-Confined High-Strength Concrete.
584 J. Compos Constr. 2014;18(4):04013058.
585 [44] Mandal S, Hoskin A, Fam A. Influence of concrete strength on confinement effectiveness
586 of fiber-reinforced polymer circular jackets. ACI Struct J. 2005;102(3):383.
587 [45] Afifi MZ, Mohamed HM, Benmokrane B. Axial Capacity of Circular Concrete Columns
588 Reinforced with GFRP Bars and Spirals. J. Compos Constr. 2014;18(1):04013017.
589 [46] ACI. Guide for the Design and Construction of Externally Bonded FRP Systems for
590 Strengthening Concrete Structures. 2008. ACI 440.2 R-08. American Concrete Institute.
591 [47] Benzaid R, Mesbah H, Chikh NE. FRP-confined concrete cylinders: axial compression
592 experiments and strength model. J Reinforced plastics and composites. 2010;29(16):2469-88.
593 [48] Harries KA, Kharel G. Behavior and modeling of concrete subject to variable confining
594 pressure. Mater J. 2002;99(2):180-9.
595 [49] Wu G, Lü Z, Wu Z. Strength and ductility of concrete cylinders confined with FRP
596 composites. Constr Build Mater. 2006;20(3):134-48.
597 [50] Youssef MN, Feng MQ, Mosallam AS. Stress–strain model for concrete confined by FRP
598 composites. Compos B: Eng. 2007;38(5-6):614-28.

599 [51] Samaan M, Mirmiran A, Shahawy M. Model of concrete confined by fiber composites. J.
600 Struct. Eng. 1998;124(9):1025-31.
601 [52] Toutanji H. Stress-strain characteristics of concrete columns externally confined with
602 advanced fiber composite sheets. ACI Mater. J. 1999;96(3):397-404.
603 [53] Lam L, Teng JG. Design-oriented stress–strain model for FRP-confined concrete. Constr.
604 Build. Mater. 2003;17(6-7):471-89.
605 [54] Teng JG, Huang YL, Lam L, Ye LP. Theoretical model for fiber-reinforced polymer-
606 confined concrete. J. Compos. Constr. 2007;11(2):201-10.

607 Table 1: Test matrix

Group designation	Specimen designation	Longitudinal reinforcement	Lateral confinement	Concrete type	Loading eccentricity
SSO	SSO-0	Steel bars	Steel helix	OPC	0
	SSO-25				25
	SSO-50				50
	SSO-F				Flexure
SSG	SSG-0	Steel bars	Steel helix	GPC	0
	SSG-25				25
	SSG-50				50
	SSG-F				Flexure
GGO	GGO-0	GFRP bars	GFRP tube	OPC	0
	GGO-25				25
	GGO-50				50
	GGO-F				Flexure
GGG	GGG-0	GFRP bars	GFRP tube	GPC	0
	GGG-25				25
	GGG-50				50
	GGG-F				Flexure

608

609

610 Table 2: Mix proportions of geopolymer concrete

Material	Quantity (kg/m^3)
Fly ash	270
GGBFS	180
Coarse Aggregates	1294
Sand	552
14 M NaOH solution	45
Na_2SiO_3	113
Water	92
Superplasticizer	35

611

612 Table 3: Test results of the specimens tested under concentric and eccentric axial loads

Specimen designation	Peak axial load (kN)	Axial deformation at peak axial load (mm)	Lateral deformation at peak axial load (mm)	Ductility index (μ)
SSO-0	1448	2.6	-	2.32
SSO-25	951	2.5	2.0	1.50
SSO-50	537	3.3	4.8	1.27
SSG-0	1946	3.4	-	1.71
SSG-25	1207	2.8	2.4	1.09
SSG-50	694	2.6	3.2	1.07
GGO-0	2631	12.9	-	3.57
GGO-25	1402	8.2	14.3	3.59
GGO-50	875	11.8	23.7	5.06
GGG-0	2283	10.4	-	3.24
GGG-25	1354	11.4	26.6	3.38
GGG-50	826	10.5	23.8	5.04

613

614 Table 4: Test results of the specimens tested under four-point bending test

Specimen designation	Peak load (kN)	Midspan deflection at peak load (mm)	Ductility index (μ)
SSO-F	233	25.8	11.7
SSG-F	239	5.4	9.3
GGO-F	569	20.7	1.7
GGG-F	327	23.8	2.2

615

Table 5: Comparison of confinement models

Model	Specimen				
	GGO-0		GGG-0		
	Predicted load P (kN)	P/P_{exp}	Predicted load P (kN)	P/P_{exp}	MAPE
ACI 440.2R-08 [46]	2160	0.82	2275	0.99	9.1
Benzaid et al. [47]	2149	0.82	2264	0.99	9.6
Harries and Kharel [48]	2028	0.77	2143	0.94	14.5
Wu et al. [49]	2095	0.80	2210	0.97	11.8
Youssef et al. [50]	1973	0.75	2079	0.91	16.9
Samaan et al. [51]	2353	0.89	2468	1.08	9.3
Toutanji [52]	2734	1.04	2866	1.26	14.7
Lam and Teng [53]	2192	0.83	2307	1.01	8.8
Teng et al. [54]	2230	0.85	2345	1.03	8.9

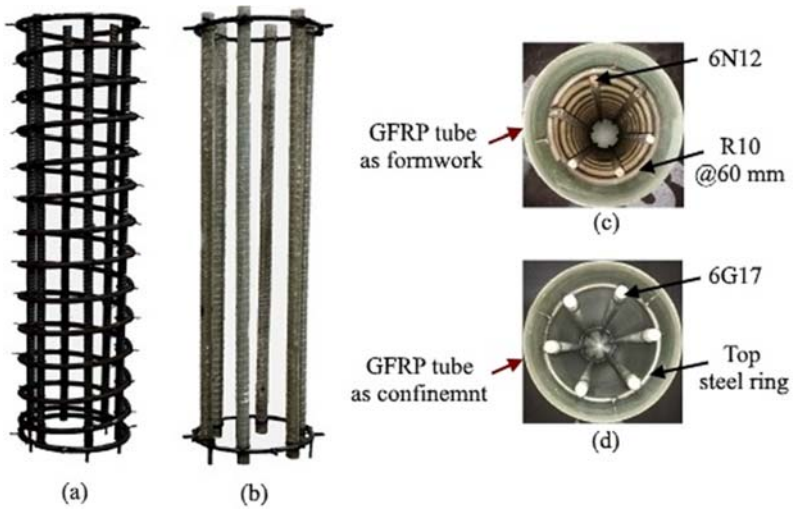

618

619 Fig. 1: Configuration of groups: (a) SSO and SSG cages; (b) GGO and GGG cages; (c) top

620 view of SSO and SSG; and (d) top view of GGO and GGG

621

622

623

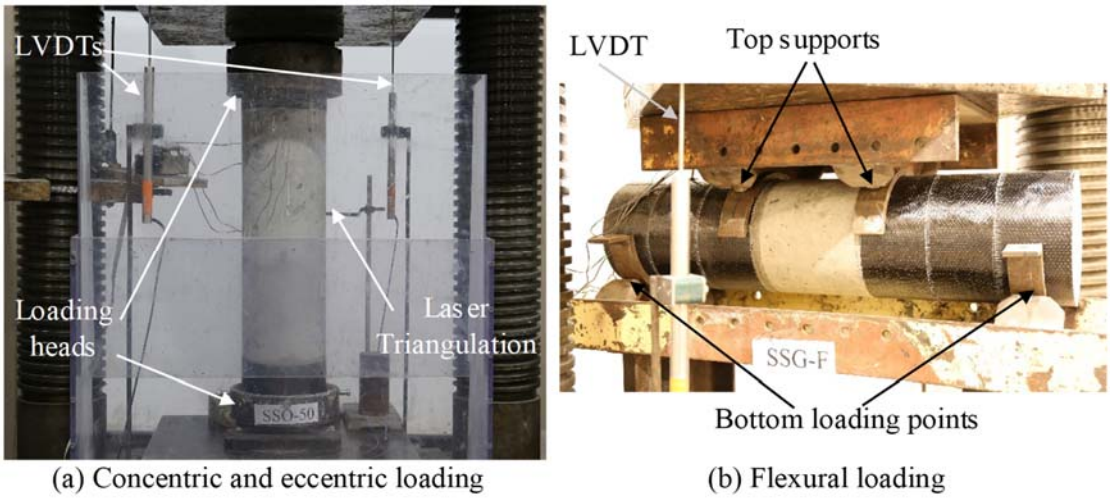

624

625 Fig. 2: Test setup for different loading types

626

(a) Specimens under concentric axial load

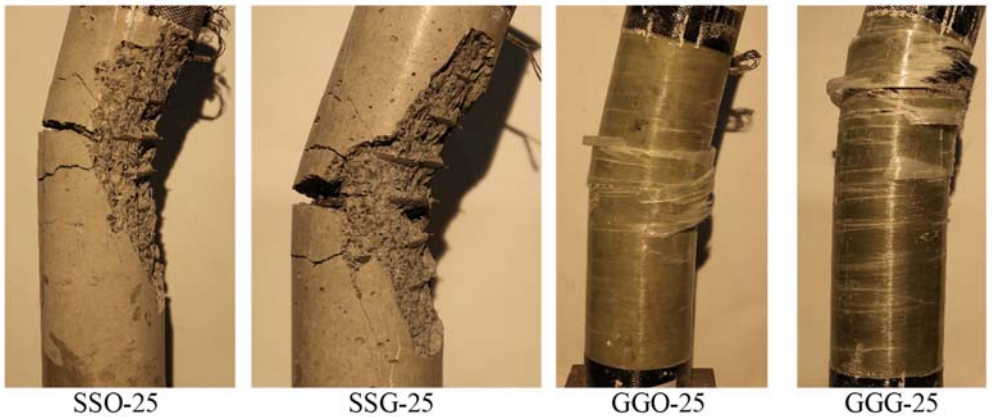

(b) Specimens under 25 mm eccentric axial load

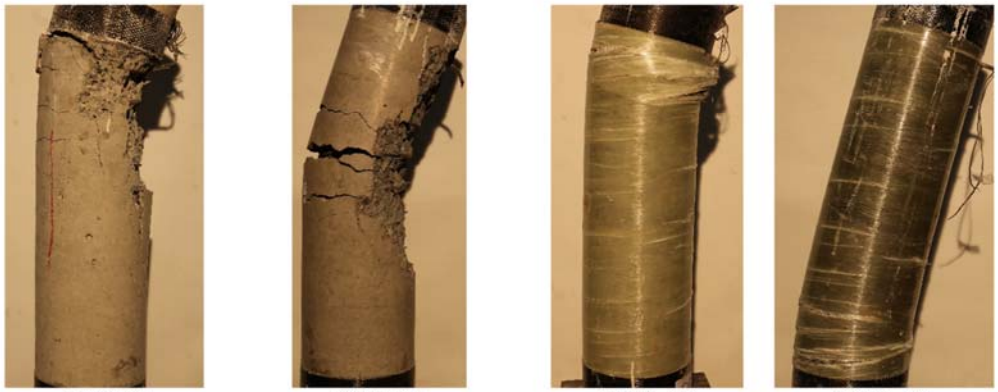

(c) Specimens under 25 mm eccentric axial load

627

628 Fig. 3: Failure modes of the test specimens tested under concentric, 25 mm eccentric and 50
629 mm eccentric loads

630

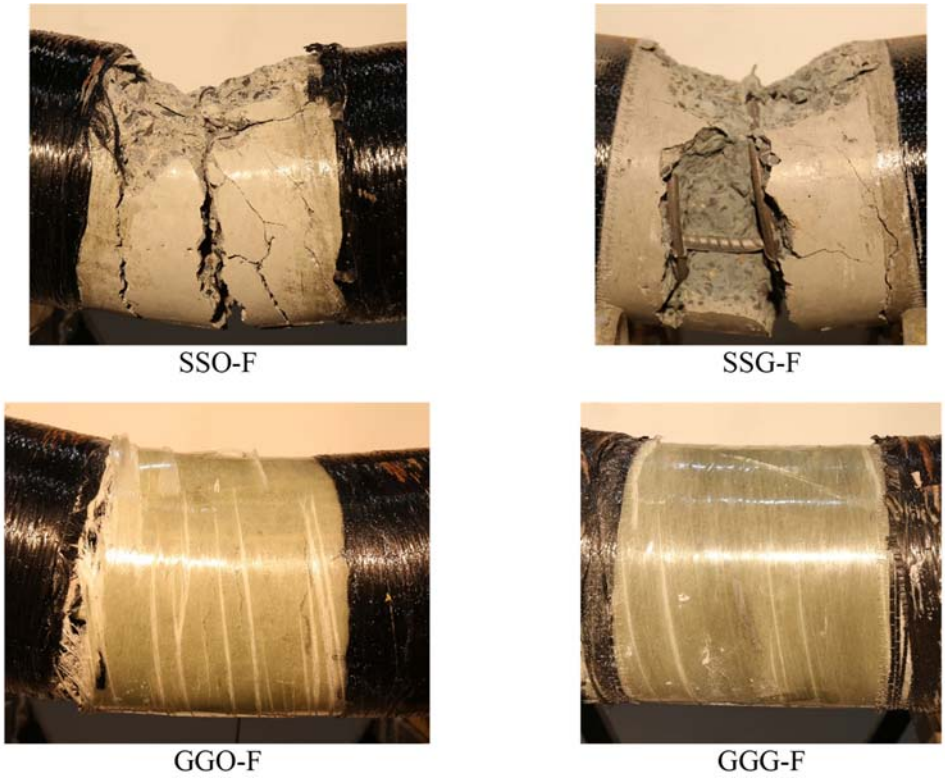

631

632 Fig. 4: Failure modes of the test specimens tested under four-point bending loads.

633

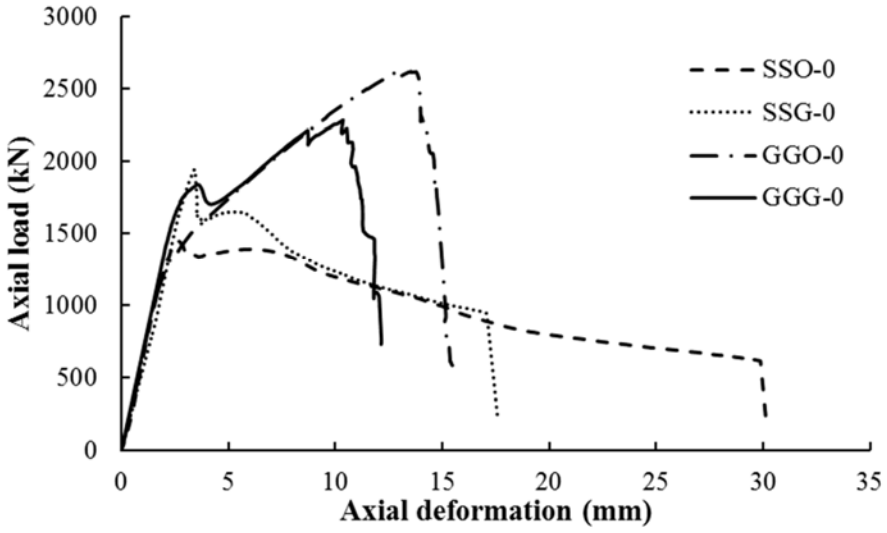

634

635 Fig. 5: Axial load-axial deformation curves for the specimens tested under concentric loads.

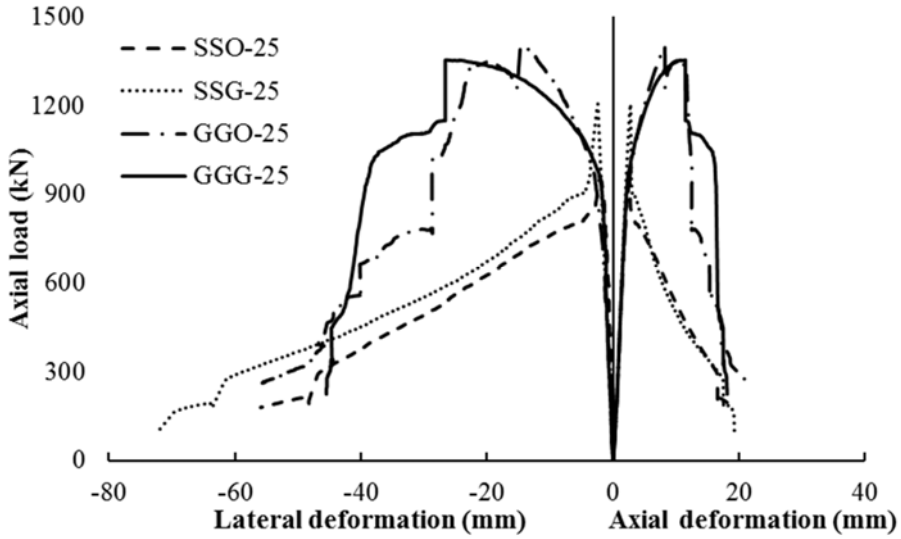

636

637 Fig. 6: Axial load-deformation behavior of the specimens tested under 25 mm load

638 eccentricity.

639

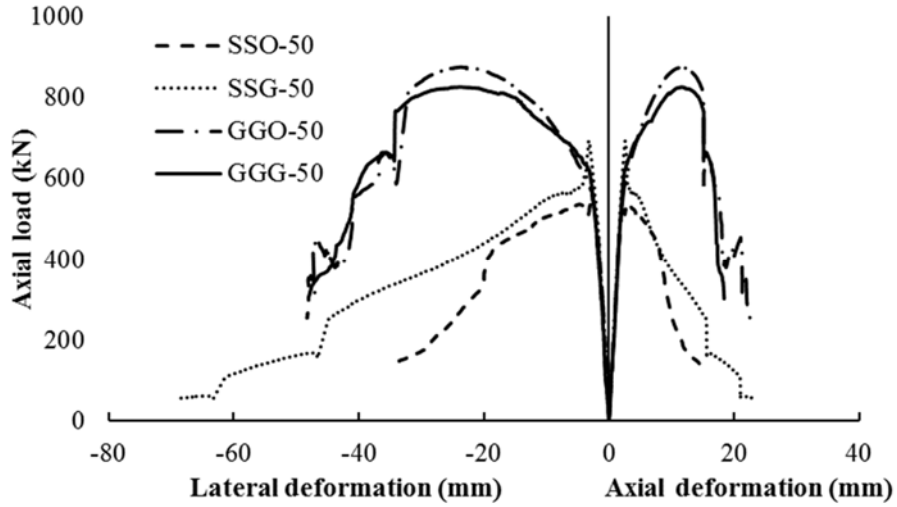

640

641 Fig. 7: Axial load-deformation behavior of the specimens tested under 50 mm load

642 eccentricity.

643

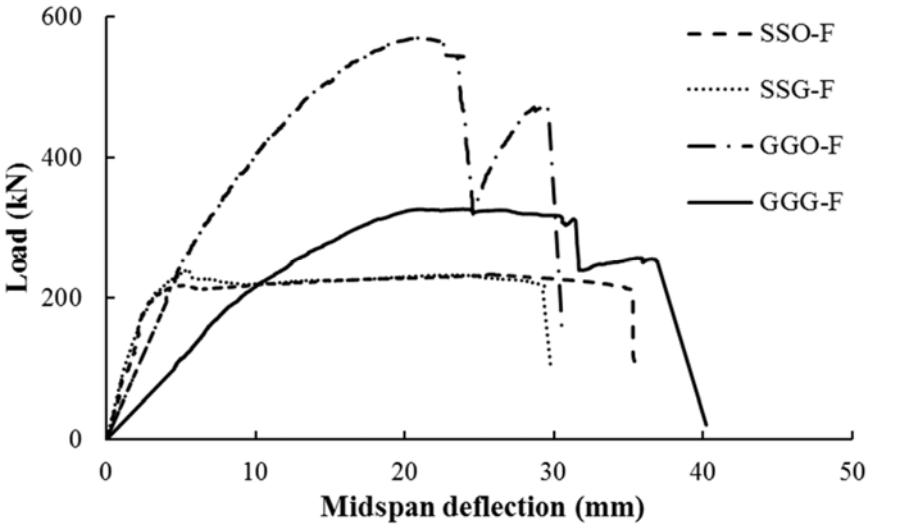

644 Fig. 8: Load-midspan deflection behavior of the specimens tested under flexural loads.

645

646

647

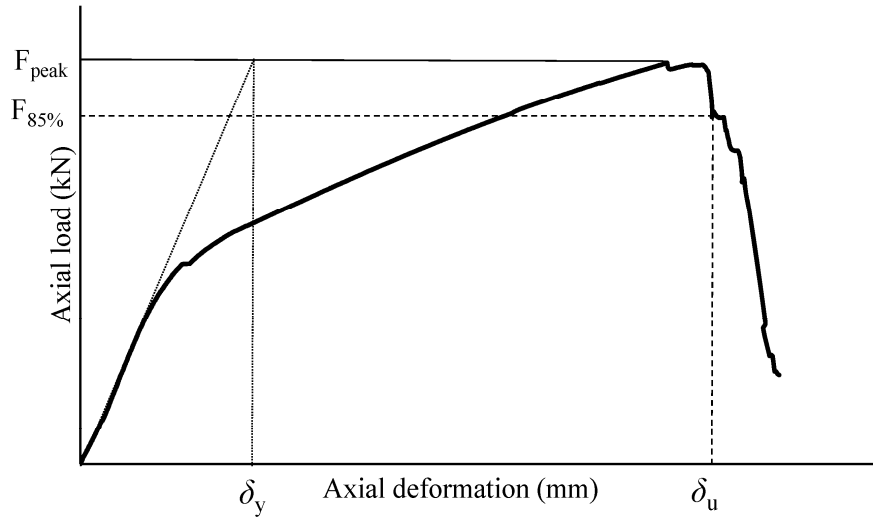

648

649 Fig. 9: Locations of ultimate and yield deformations for ductility index calculations.

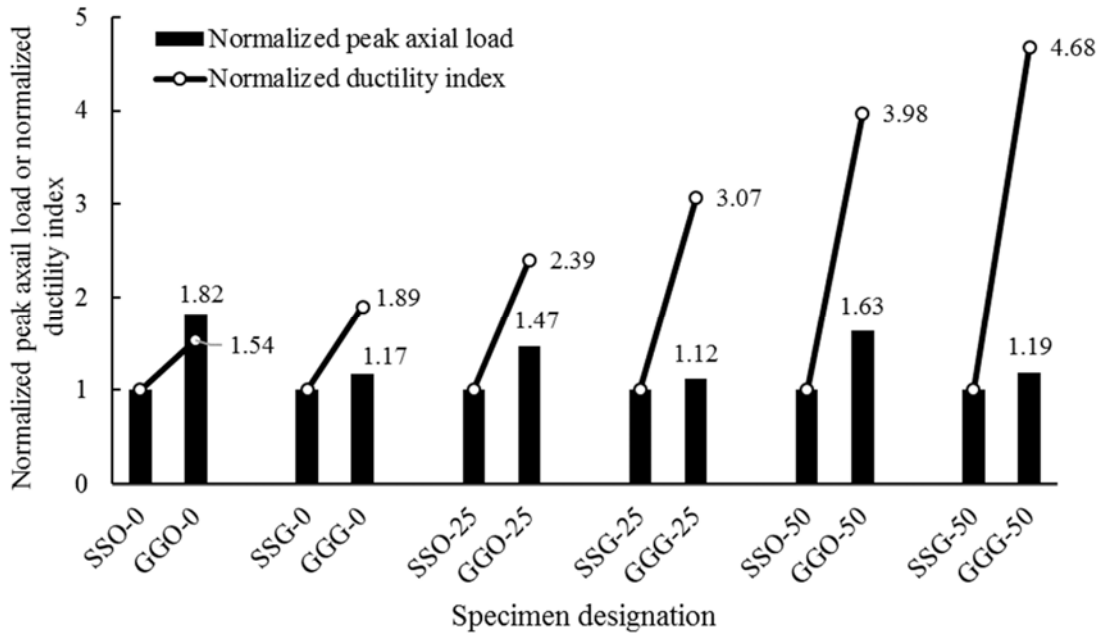

650

651 Fig. 10: Effect of longitudinal reinforcement and transverse confinement on peak axial load

652 and ductility index.

653

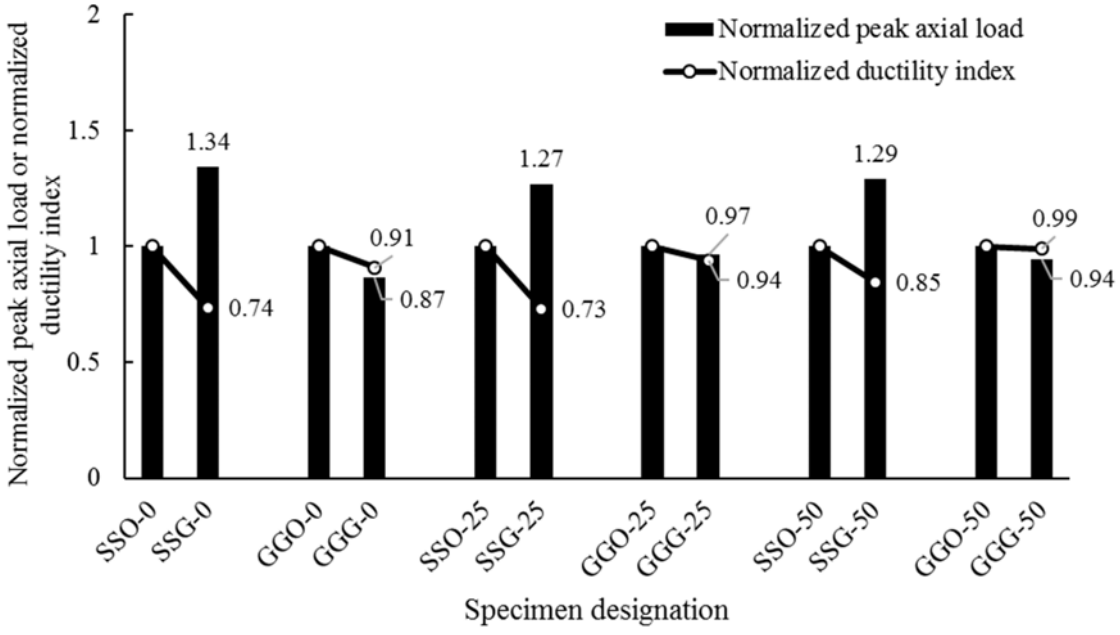

654

655 Fig. 11: Effect of concrete type on peak axial load and ductility index.

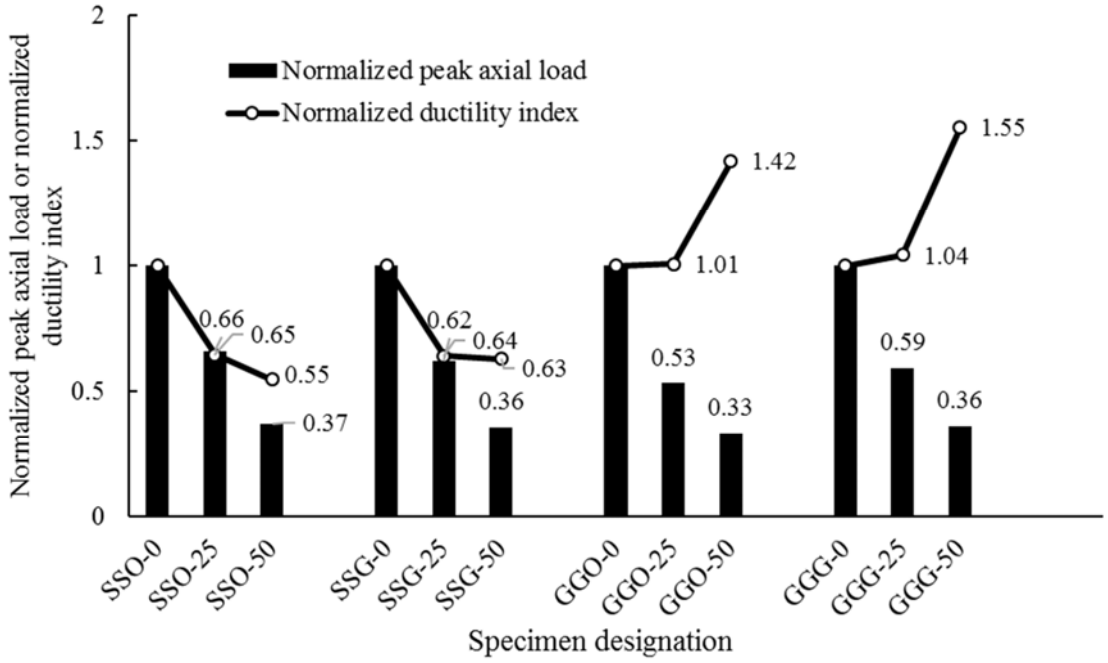

Fig. 12: Effect of load eccentricity on peak axial load and ductility index.